



Forschungszentrum Karlsruhe
in der Helmholtz-Gemeinschaft

Wissenschaftliche Berichte
FZKA 6938

Stress Intensity Factors and Constant Stress Terms for Interface Cracks

T. Fett, G. Rizzi

Institut für Materialforschung

Januar 2004

FORSCHUNGSZENTRUM KARLSRUHE

in der Helmholtz-Gemeinschaft

Wissenschaftliche Berichte

FZKA 6938

**STRESS INTENSITY FACTORS AND
CONSTANT STRESS TERMS FOR
INTERFACE CRACKS**

T. Fett, G. Rizzi

Institut für Materialforschung

Forschungszentrum Karlsruhe GmbH, Karlsruhe

2004

Impressum der Print-Ausgabe:

**Als Manuskript gedruckt
Für diesen Bericht behalten wir uns alle Rechte vor**

**Forschungszentrum Karlsruhe GmbH
Postfach 3640, 76021 Karlsruhe**

**Mitglied der Hermann von Helmholtz-Gemeinschaft
Deutscher Forschungszentren (HGF)**

ISSN 0947-8620

Stress intensity factors and constant stress terms for interface cracks

Abstract:

In bi-material joints cracks can propagate along the interface or kink into one of the two materials. Whereas the energy release rate can be applied for interface cracks in the same way as usual for homogeneous materials, the computation of stresses in the vicinity of the crack tip is significantly more complicated. In order to assess crack kinking, it is necessary to know the mixed-mode stress intensity factor contributions K_I and K_{II} as well as the constant stress terms in the two materials.

Whereas the stress intensity factors are available for a large number of infinite and semi-infinite bodies, there is experimental interest in practically used test specimens. This especially holds for the constant α -stress terms.

Finite element computations are performed for the special case of a disappearing second Dundurs parameter, i.e. $\beta=0$. The fracture mechanics parameters K_I , K_{II} , σ_0 for the interface crack are reported in the form of diagrams and approximate relations.

Spannungsintensitätsfaktoren und Konstantspannung für Grenzflächenrisse

Kurzfassung:

In Materialverbunden können sich Risse entlang der Verbindungsfläche ausbreiten oder aber in eines der beiden Materialien abknicken. Während die Ausbreitung in Interface-Richtung wie auch bei homogenen Materialien durch die Energiefreisetzungsrates beschrieben werden kann, erfordert die Bewertung des Abknickverhaltens die Kenntnis der Spannungen vor der Risspitze. Deren Ermittlung ist relativ kompliziert. Die notwendigen bruchmechanischen Belastungsgrößen sind die Mode-I- und Mode-II-Spannungsintensitätsfaktoren K_I und K_{II} sowie die ersten regulären Spannungsterme in den beiden Materialien.

Ziel des Berichts ist die Ermittlung dieser Größen für den Spezialfall verschwindenden zweiten Dundurs-Parameters ($\beta=0$) mit der Methode der Finiten Elemente.

Contents

1. Introduction	
1.1 Interface crack	1
1.2 Kink	2
2. Double Cantilever Beam	4
2.1 Computations for a slender DCB specimen	4
2.1.1 Energy release rate and effective stress intensity factor	4
2.1.2 Mixed-mode stress intensity factors	5
2.1.3 Constant stress terms	6
2.2 Influence of the a/d -ratio	8
2.2.1 Energy release rate	8
2.2.2 Mixed-mode stress intensity factors	9
2.2.3 Constant stress terms	11
3. The CT-specimen	13
3.1 Mixed-mode stress intensity factors	13
3.2 Constant stress terms	15
4. DCDC-test specimen	17
5. Opposite roller test	20
6. Bending test	24
References	28

1. Introduction

The mechanical behaviour of a bi-material joint (consisting of materials “1” and “2”) is characterised by the Dundurs parameters α and β which are defined as

$$\alpha = \frac{\bar{E}_1 - \bar{E}_2}{\bar{E}_1 + \bar{E}_2}, \quad \bar{E} = \frac{E}{1 - \nu^2} \quad (1)$$

$$\beta = \frac{1}{2} \frac{\mu_1(1 - 2\nu_2) - \mu_2(1 - 2\nu_1)}{\mu_1(1 - \nu_2) + \mu_2(1 - \nu_1)}, \quad \mu = \frac{E}{2(1 + \nu)} \quad (2)$$

with Young’s modulus E and Poisson’s ratio ν .

1.1 Interface crack

For a crack lying directly on the interface (Fig. 1), the stress field is given by a complex interface stress intensity factor K [1] expressed as

$$K = K_1 + iK_2 \quad (3)$$

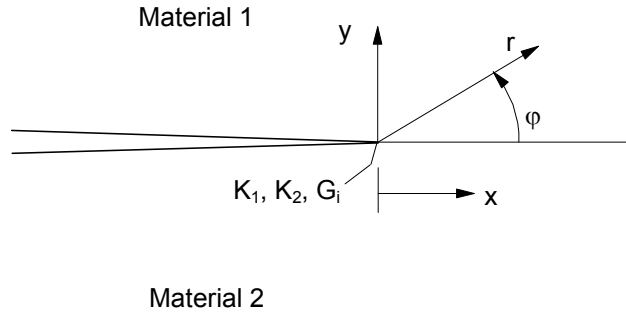


Fig. 1 Interface crack (geometric data).

The full stress solution for such cracks was given by Sih and Chen [2]. The tractions on the interface ahead of the crack tip ($r \rightarrow x$, $\varphi=0$) are

$$\sigma_{22} + i\sigma_{12} = \frac{K}{\sqrt{2\pi x}} x^{i\varepsilon} \quad (4)$$

with

$$\varepsilon = \frac{1}{2\pi} \ln \frac{1 - \beta}{1 + \beta} \quad (5)$$

The energy release rate G for an advance of the crack in the interface direction reads

$$G = \frac{K_1^2 + K_2^2}{E^*} \quad (6)$$

with the effective modulus E^* defined as

$$\frac{1}{E^*} = \frac{1}{2} \left(\frac{1}{E_1} + \frac{1}{E_2} \right) \frac{1}{\cosh^2 \pi \varepsilon} \quad (7)$$

As can be seen from (6) and (7) the energy release rate can be applied for interface cracks in the same way as usual for homogeneous materials. If the stresses in the vicinity of the crack tip are of interest, the computations are significantly more complicated. Knowledge of these stresses is necessary to decide whether a crack will extend in its initial direction (i.e. on the interface) or kink into one of the two materials [3].

When $\beta=0$, and consequently $\varepsilon=0$, the stress intensity factors K_1 and K_2 can be interpreted as conventional stress intensity factors K_I and K_{II} ($K_1 \rightarrow K_I$, $K_2 \rightarrow K_{II}$).

1.2 Kink crack

The conditions of kinking are outlined in detail in the papers of He and Hutchinson [3] and He et al.[4]. The stress intensity factors of the kinked crack (Fig. 2) k_I and k_{II} are conventional stress intensity factors, because the crack tip is now surrounded by one material exclusively. These stress intensity factors are related to the stress intensity factors of the unkinked crack as well as to the constant stress term σ_0 in the material in which the crack will kink

$$k_I + ik_{II} = cK\ell^{i\varepsilon} + d\bar{K}\ell^{-i\varepsilon} + b\sigma_0\sqrt{\ell} \quad (8)$$

where c , d , and b are dimensionless complex parameters depending on the Dundurs parameters and the kink angle ω . In the case of Fig. 2, the relevant constant stress term is σ_{02} . For homogeneous materials the stress σ_0 is identical with the so-called T-stress. The effects of T on path stability under mixed-mode loading were discussed in detail by Cotterell and Rice [5].

For the special case of $\beta=0$, the stress intensity factors for the kink are

$$k_I = (c_R + d_R)K_1 - (c_I + d_I)K_2 + b_1\sigma_0\sqrt{\ell} \quad (9)$$

$$k_{II} = (c_I - d_I)K_1 + (c_R - d_R)K_2 + b_2\sigma_0\sqrt{\ell} \quad (10)$$

The energy release rate G_k for the kink crack then results from

$$G_k = \frac{k_I^2 + k_{II}^2}{E_2} \quad (11)$$

The a priori unknown kink angle ω can be determined from eq.(11) taking $\ell \rightarrow 0$. The ratio of the interface energy release rate G_i and the maximum value of $G_k(\omega)$ under kink conditions, $G_{k,\max}$, have to be determined. The value of $G_i/G_{k,\max}$ obtained can then be compared with the ratio of the mode-dependent interface toughness Γ_i and the toughness of the ma-

terial in which the crack kinks, Γ_k , i.e. Γ_i/Γ_k . This allows to decide whether the crack is able to kink (for details see [4]).

In order to model the crack growth and kink behaviour of interface cracks, it is necessary to determine the stress intensity factors K_I , K_{II} (or K_I and K_{II} , for $\beta=0$) and the constant stress terms for the specimens of interest. Whereas the stress intensity factors are available for a large number of infinite and semi-infinite bodies (see e.g.[6]), there is experimental interest in practically used test specimens. This especially holds for the constant x-stress terms.

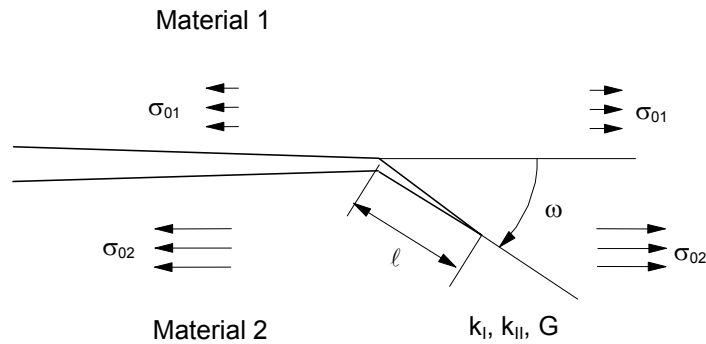


Fig. 2 Geometry of a kinked crack with constant stress terms of the initial (unkinked) crack.

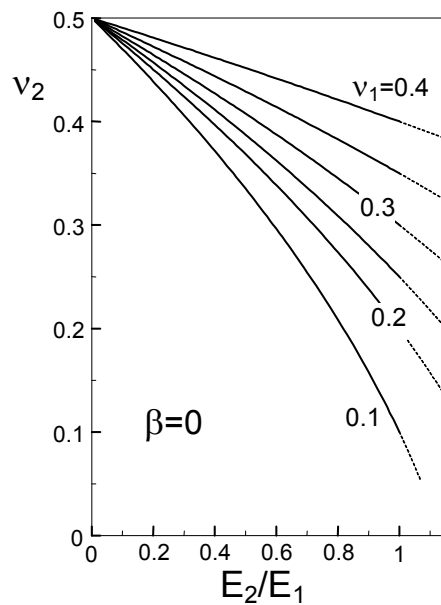


Fig. 3 Poisson's ratio v_2 required for a disappearing Dundurs parameter β .

As emphasized by Hutchinson [7], “the clarity in interpretation achieved by taking β to be zero is often worth the small sacrifice in accuracy” [2]. Having this in mind, the special case of $\beta=0$ will be considered in detail below. For a given ratio of Young's modulus E_2/E_1 and a prescribed Poisson ratio v_1 , the second Poisson ratio that fulfils $\beta=0$, is given as

$$\nu_2 = -\frac{1}{4} + \sqrt{\frac{9}{16} - \frac{1}{2}(1 - \nu_1 - 2\nu_1^2)E_2 / E_1} \quad (12)$$

Figure 3 represents this dependency for several values of ν_1 .

2. Double Cantilever Beam

The double-cantilever-beam (DCB) specimen is shown in Fig. 4. A line load P/B (B =specimen thickness, often chosen as $B=1$) is applied at the end of the cantilever normally to the crack face.

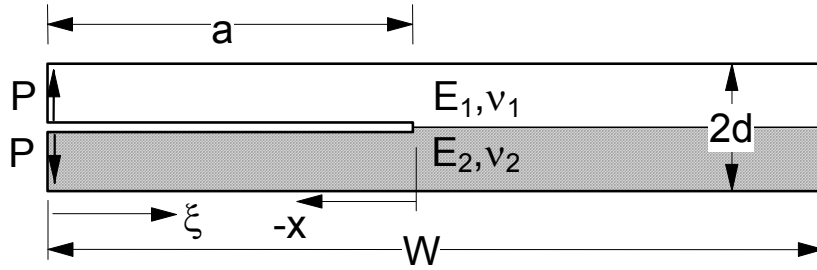


Fig. 4 Double-cantilever-beam specimen made of dissimilar materials.

Finite element (FE) computations were carried out with ABAQUS Version 6.2 which provides the stress intensity factors K_I as well as the energy release rate in the form of the J-integral. For the FE computations the geometry was chosen to be $W=6000$ and $d=500-1500$. In total, about 7400 elements with 23000 nodes were used. The crack tip region was modelled with 8-node isoparametric elements collapsed on one side.

2.1 Computations for a slender DCB specimen ($d/W=12$)

2.1.1 Energy release rate and effective stress intensity factor

The energy release rate was determined as a function of the first Dundurs parameter α . By use of eqs.(6) and (7), an effective stress intensity factor K_{eff} can be defined as

$$K_{eff} = \sqrt{GE^*} \quad (13)$$

with the effective Young's modulus E^* given by eq.(7). The results for $a/d=6$ are represented in this form in Fig. 5. There is no significant dependency on α (this had to be expected). The solid and dashed horizontal lines indicate the average value and the span of data, i.e. $K_{eff}\sqrt{d}/(P/B)=23.08 (\pm 0.3\%)$. Such small deviations are within the range of accuracy of the FE method.

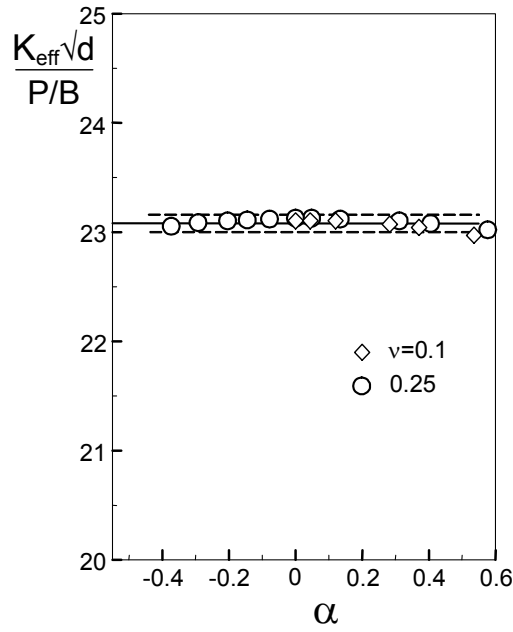


Fig. 5 Energy release rate G for the advance of an interface crack expressed by the effective stress intensity factor according to eq.(13) for $a/d=6$ and $\beta=0$.

2.1.2 Mixed-mode stress intensity factors

Mixed-mode stress intensity factors K_I and K_{II} are plotted in Fig. 6 as functions of the modulus ratio E_2/E_1 . Maximum K_I and trivially disappearing K_{II} are found for $E_2/E_1=1$. Only a slight influence of ν_1 is visible. Figure 7 shows similar plots for the dependency on the Dundurs parameter α .

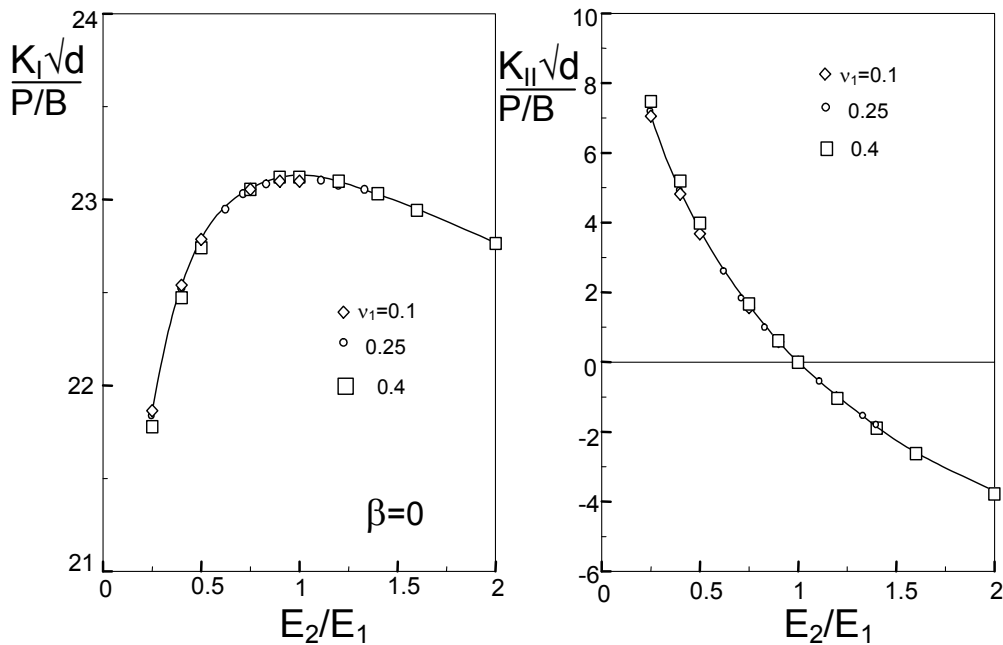


Fig. 6 Stress intensity factor contributions for $a/d=6$ ($\beta=0$).

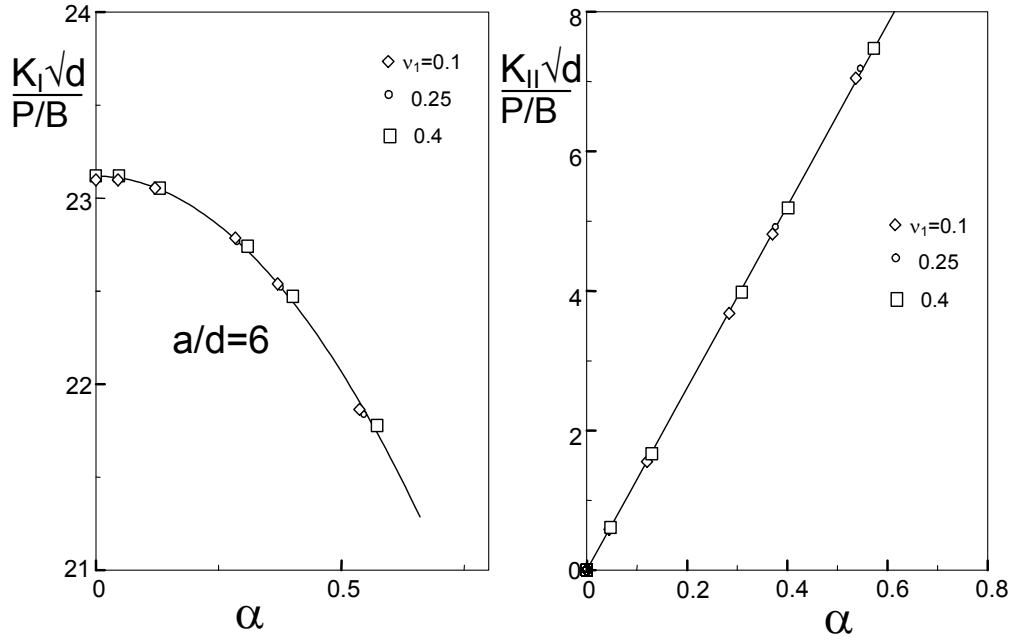


Fig. 7 Stress intensity factors K_I and K_{II} as functions of the first Dundurs parameter α for $a/d=6$ ($\beta=0$).

2.1.3 Constant stress terms

In homogeneous materials, only one constant stress term exists, the T-stress. This value can be determined easily from the x-stresses at the free crack surfaces, as there is no other stress component near the crack tip. Moreover, the ABAQUS Version 6.2 directly provides T .

In the case of an interface crack, two different values exist for the constant x-stress term, here denoted as σ_{01} for material “1” and σ_{02} for material “2”. Their determination requires a least-squares evaluation procedure. Whereas for pure mode-I stress fields the singular stresses vanish at $\varphi = \pm \pi$, the mode-II stress intensity factor yields singular x-stresses also at the crack surface under mixed-mode conditions. The total stresses caused by the mode-II stress intensity factor and the constant stress terms are

$$\sigma_x = -\frac{K_{II}}{\sqrt{2r\pi}} (2 + \cos \frac{1}{2} \varphi \cos \frac{3}{2} \varphi) \sin \frac{1}{2} \varphi + \sigma_0 \quad (14)$$

The x-stresses at the crack faces ($\varphi = \pm \pi$) reads

$$\sigma_x = -\frac{2K_{II}}{\sqrt{-2x\pi}} + \sigma_0 \quad (15)$$

For the evaluation of σ_0 , eq.(15) may be rewritten as

$$\sigma_x \sqrt{-x} = -\frac{\sqrt{2}K_{II}}{\sqrt{\pi}} + \sigma_0 \sqrt{-x} \quad (16)$$

The constant stress is then determined from the slope of a $\sigma_x\sqrt{-x}$ versus $\sqrt{-x}$ plot, as shown in Fig. 8 for $a/d=6$ and two different ratios of Young's modulus. The values at $\sqrt{-x}=0$ provide the mode-II stress intensity factor.

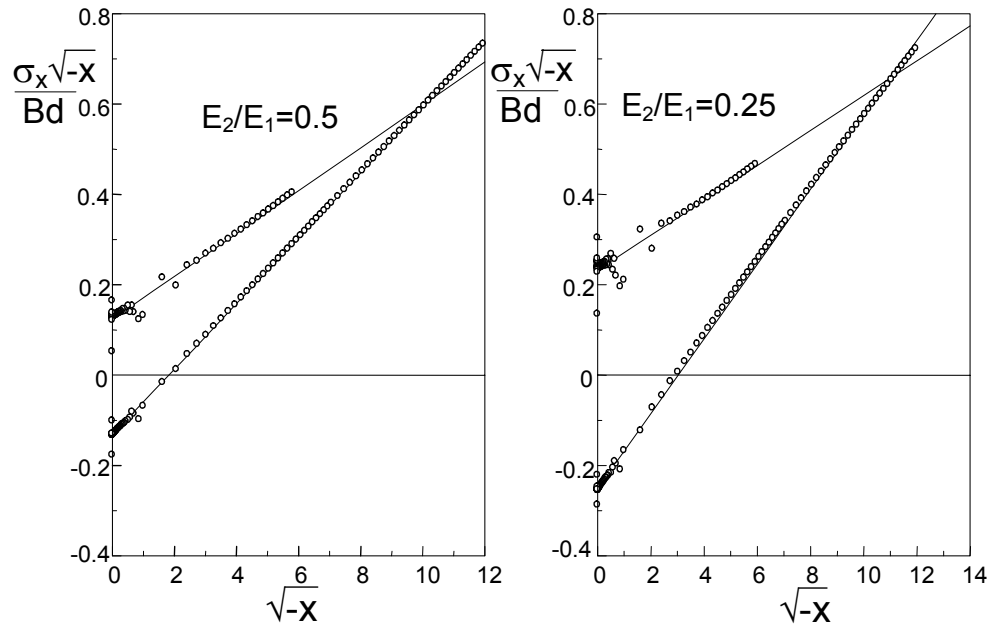


Fig. 8 Determination of the constant stress terms from the slope of the straight lines ($\beta=0$).

Figure 9 shows the constant stress terms as functions of the Young's modulus ratio E_2/E_1 . A plot of σ_0 versus the Dundurs parameter α is shown in Fig. 10. A straight-line behaviour can be concluded.

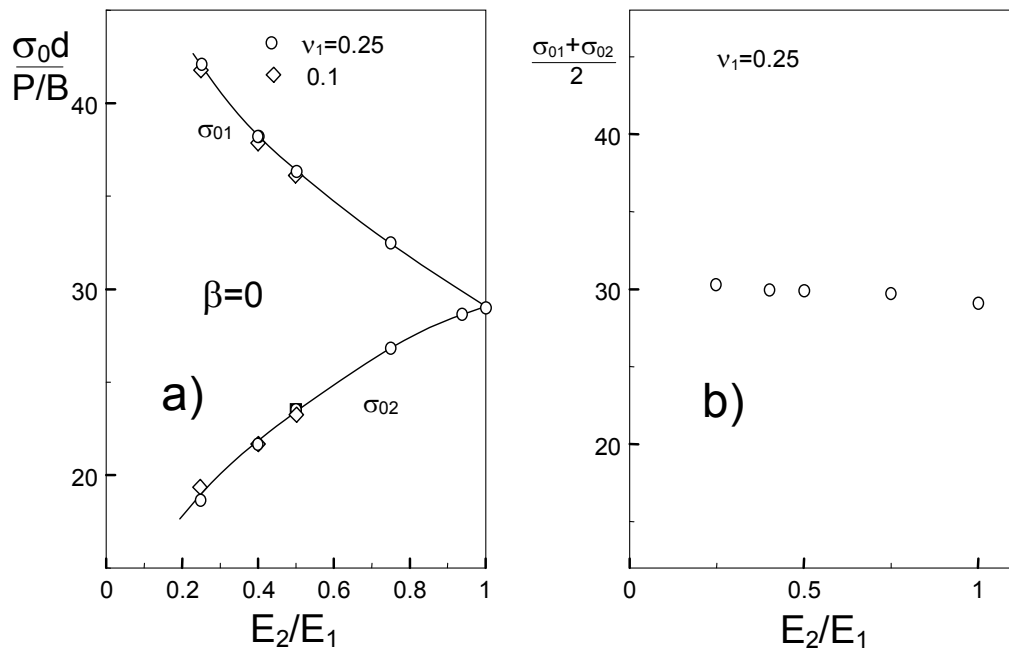


Fig. 9 a) Constant stress terms versus ratio E_2/E_1 , b) average of the two constant stress values σ_{01} and σ_{02} ($a/d=6$, $\beta=0$).

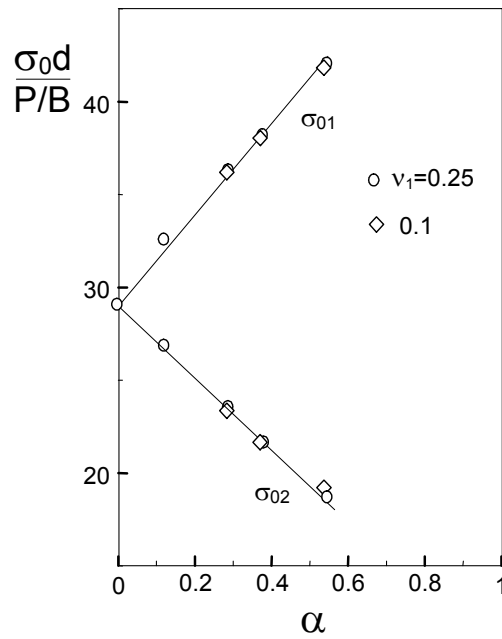


Fig. 10 Constant stress terms σ_{01} and σ_{02} as functions of the first Dundurs parameter α for $a/d=6$, $\beta=0$.

2.2 Influence of the a/d ratio

2.2.1 Energy release rate

Figure 11 shows the effective stress intensity factor according to eq.(13) for three different a/d ratios. The effective stress intensity factor increases with a/d , but is nearly independent of the parameters α and ν_1 .

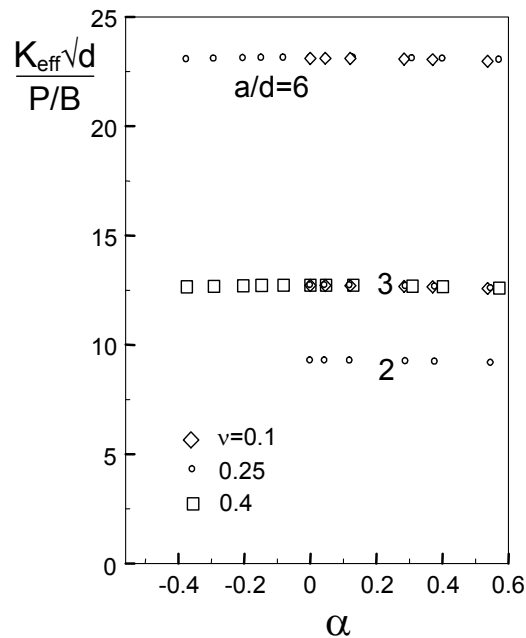


Fig. 11 Influence of the a/d ratio on the effective stress intensity factor.

2.2.2 Mixed-mode stress intensity factors

The stress intensity factor contributions K_I and K_{II} are plotted in Fig. 12 as functions of the Dundurs parameter α , the ratio a/d , and the Poisson ratio ν_1 .

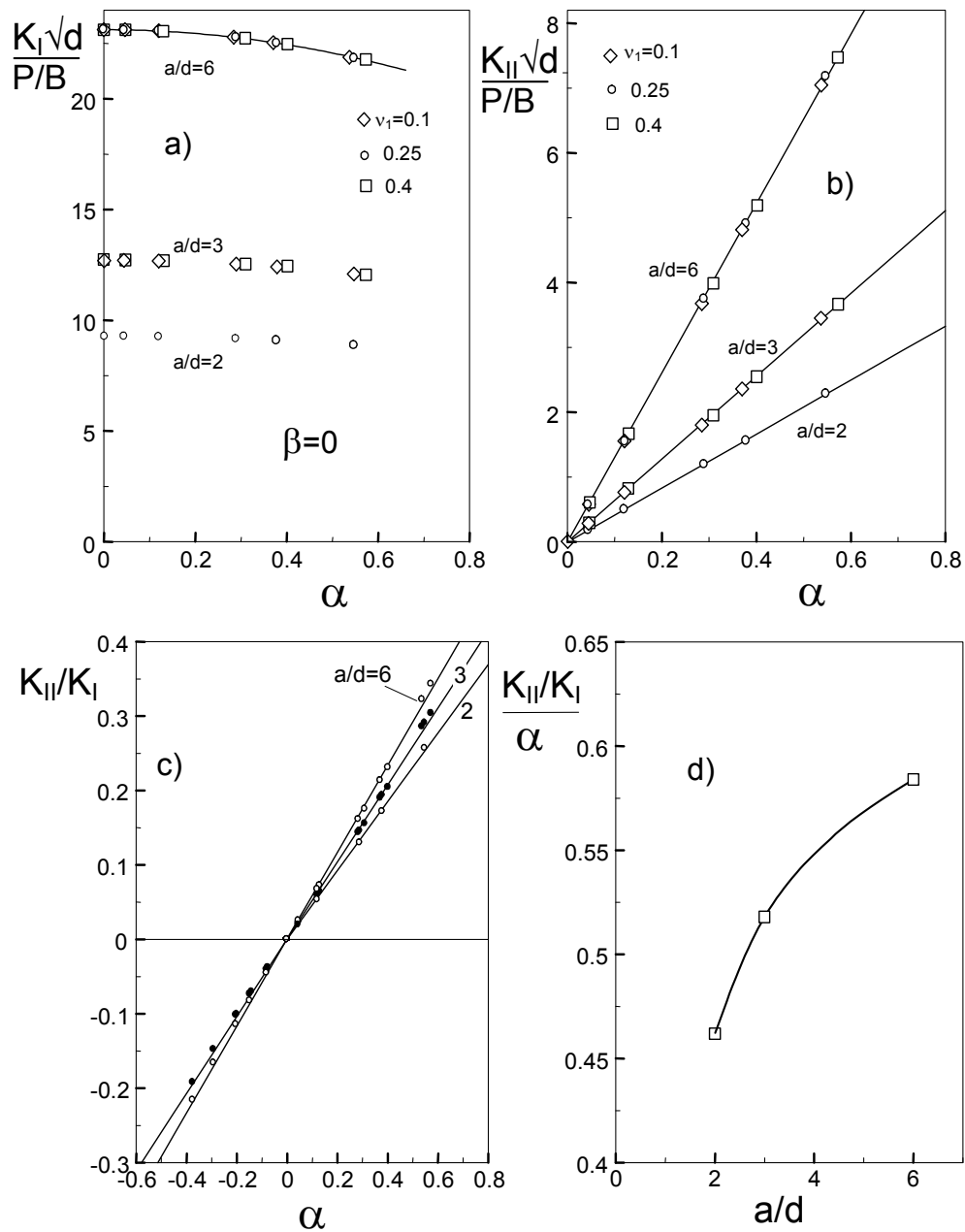


Fig. 12 Stress intensity factors K_I (a) and K_{II} (b) as functions of the first Dundurs parameter α for different a/d ($\beta=0$), c) and d): mode-mixity K_{II}/K_I .

The dependencies on α can be approximated as

$$\frac{K_I(\alpha)}{K_I(0)} \cong 1 - 0.171\alpha^2 \quad (17a)$$

and

$$K_{II}(\alpha) \propto \alpha \quad (17b)$$

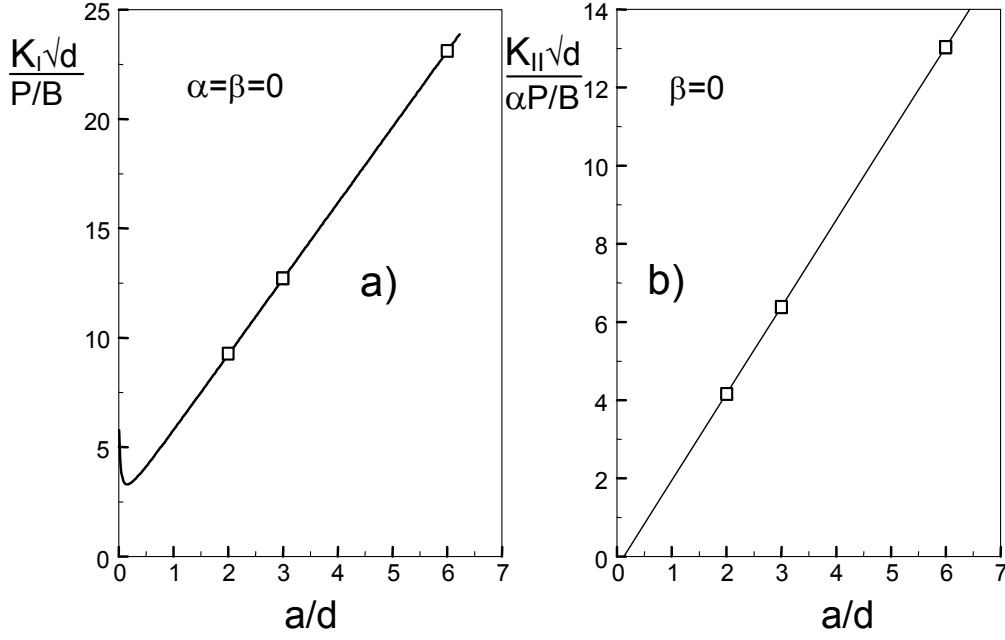


Fig. 13 a) Stress intensity factor of a homogeneous material versus a/d (curve given by eq.(19a)), b) K_{II}/α for several ratios a/d .

Figure 12c represents the “mode mixity” K_{II}/K_I . Also this quantity is found to be linearly dependent on α . The coefficient of proportionality is entered in Fig. 12d.

For the special case of a homogeneous material ($\alpha=\beta=0$), the mode-I stress intensity factor can be determined from the weight function which reads [8]

$$h = \sqrt{\frac{12}{d}} \left(\frac{a-\xi}{d} + \lambda \right) + \sqrt{\frac{2}{\pi(a-\xi)}} \exp\left(-\sqrt{12} \frac{a-\xi}{d} \right) \quad (18)$$

with $\lambda=0.68$. The stress intensity factor for loading at $\xi=0$ then results as

$$\frac{K_I}{P/B} = \sqrt{\frac{12}{d}} \left(\frac{a}{d} + \lambda \right) + \sqrt{\frac{2}{\pi a}} \exp\left(-\sqrt{12} \frac{a}{d} \right) \quad (19a)$$

This solution is introduced in Fig. 13a as the curve. Equation (19a) may be simplified for $a/d > 1$ by

$$K_I \cong \frac{P}{B} \sqrt{\frac{12}{d}} \left(\frac{a}{d} + \lambda \right) \quad (19b)$$

Together with eq.(17a) the following expression is obtained for the case of dissimilar materials

$$K_I \cong \frac{P}{B} \sqrt{\frac{12}{d}} \left(\frac{a}{d} + \lambda \right) (1 - 0.171\alpha^2) \quad (20)$$

Figure 13b displays the mode-II stress intensity factor as a function of a/d . The straight line dependency (solid line) is represented by

$$K_{II} \cong \frac{P}{B\sqrt{d}} \frac{20}{9} \left(\frac{a}{d} - \frac{1}{8} \right) \alpha \quad (21)$$

2.2.3 Constant stress terms

The constant stress terms σ_{01} and σ_{02} are represented in Fig. 14. These results may be approximated by the straight line relations of

$$\sigma_{01} = T(1 - \lambda\alpha) \quad , \quad 0 \leq \alpha \leq 0.5 \quad (22)$$

$$\sigma_{02} = T(1 + 0.8\alpha) \quad (23)$$

where T is the constant stress term for $\alpha=0$, i.e. the T-stress of the homogeneous specimen.

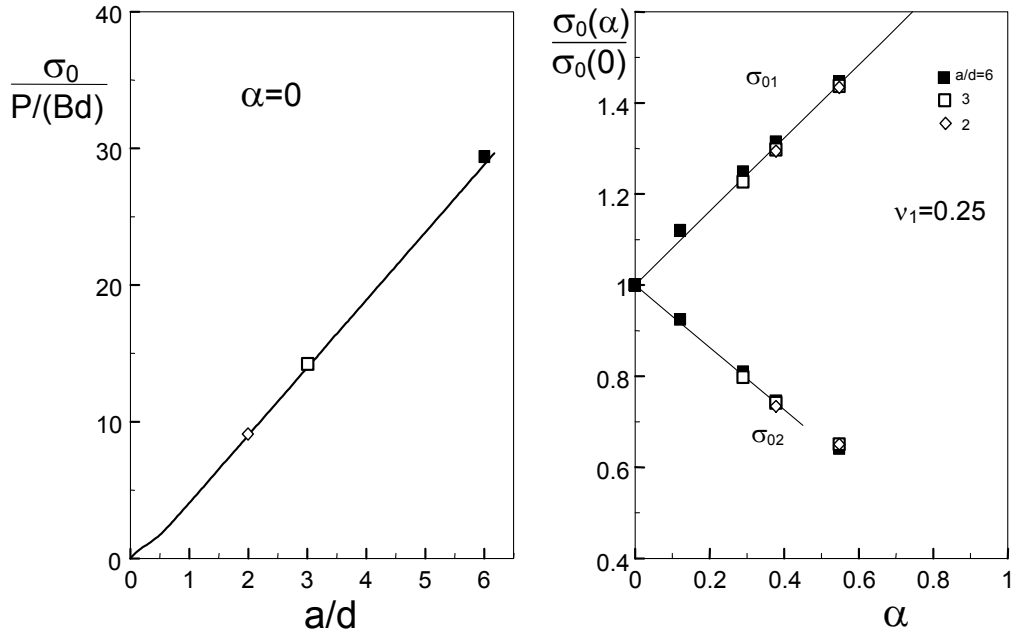


Fig. 14 a) Constant stress term of the homogeneous material versus a/d (curve given by eq.(26)), b) plot of the constant stress terms normalised to the constant stress of homogeneous material for several ratios of a/d ($\beta=0$).

The T-stress caused by a point force at the distance ξ from the end of the bar is given in [] as

$$\frac{T}{P/(Bd)} = 4.95 \frac{a - \xi}{d} - 0.9 \left[1 - \exp\left(-7.2 \frac{(a - \xi)^2}{d^2}\right) \right] \quad (24)$$

and for the special case $\xi=0$, it results

$$\frac{T}{P/(Bd)} = 4.95 \frac{a}{d} - 0.9 \left[1 - \exp\left(-7.2 \frac{a^2}{d^2}\right) \right] \quad (25)$$

or simplified for $a > d$

$$\frac{T}{P/(Bd)} \cong 4.95 \frac{a}{d} - 0.9 \quad (26)$$

Equation (25) is introduced in Fig. 14a as the solid curve.

3. The CT specimen

The standard geometry of the compact tension (CT) specimen is illustrated in Fig. 15. The thickness again is B . Computations similar to those given in detail for the DCB specimen were performed for the CT specimen. The graphical representations only concentrate on the most essential results.

3.1 Mixed-mode stress intensity factors

Figure 16 shows the mode-I stress intensity factor solution. The circles correspond to the stress intensity factor K_I and the squares represent the energy release rate expressed by eq.(13) in terms of the effective stress intensity factor K_{eff} . Figure 16b gives the data for $a/W=0.5$ in higher resolution.

From Fig. 16, it becomes obvious that

- the dependence on α is negligible and
- the effective stress intensity factor is nearly identical with the mode-I contribution.

This behaviour is due to the very small mode-II stress intensity factor contributions which are less than 10% of the mode-I stress intensity factors, as can be seen from Fig. 17a. As evident from this diagram, the dependency of K_{II} on the Dundurs parameter α is linear.

Figure 17b represents the mode mixity K_{II}/K_I . Also this plot reflects the minor influence of K_{II} for the CT specimen, as obvious from comparing with the mode mixity for the DCB specimen (Fig. 12c). Figure 17c, finally, shows the slope of the straight lines in Fig. 17b.

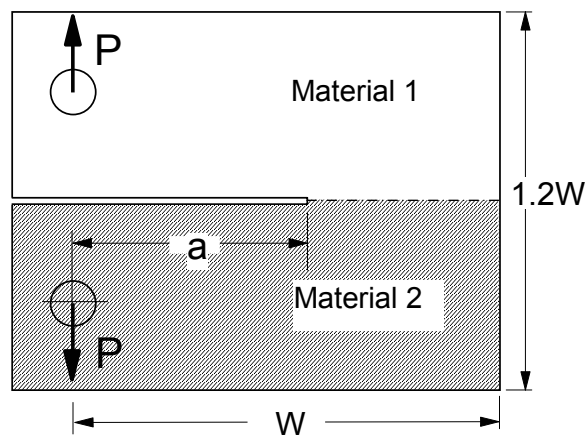


Fig. 15 The compact tension test specimen.

In Fig. 18 the stress intensity factor K_I of the homogeneous material ($\alpha=\beta=0$) is plotted versus the relative crack length a/W as the squares. The well-known stress intensity factor solution for the CT specimen made of homogeneous material is [10]

$$K_I = \frac{P}{B\sqrt{W}} \frac{(2 + \eta)(0.886 + 4.64\eta - 13.32\eta^2 + 14.72\eta^3 - 5.6\eta^4)}{(1 - \eta)^{3/2}}, \quad \eta = a/W \quad (27)$$

This dependency is also represented as the curve in Fig. 18a. Good agreement is obvious.

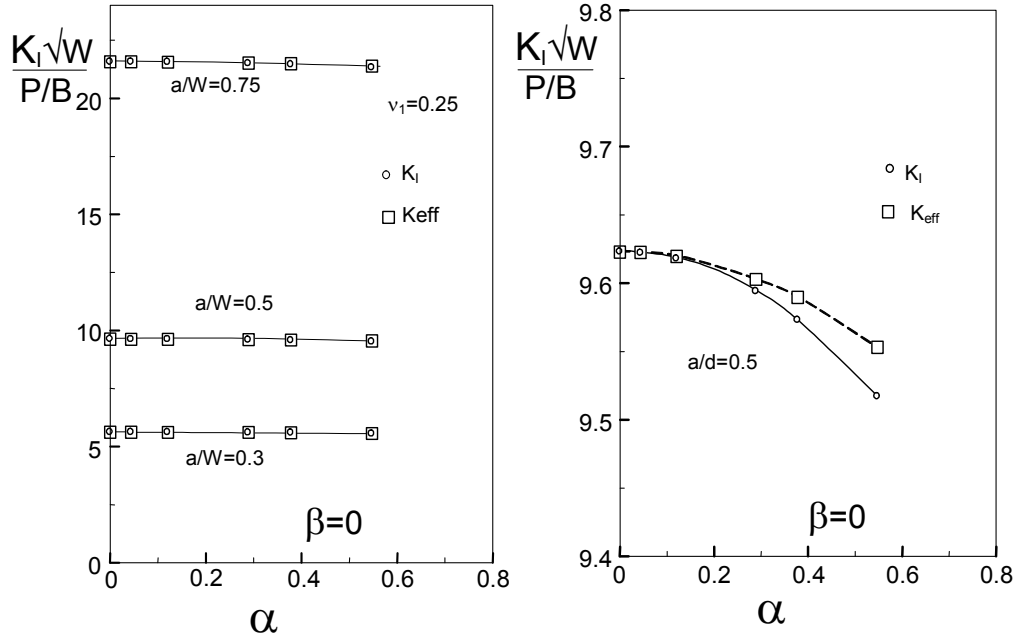
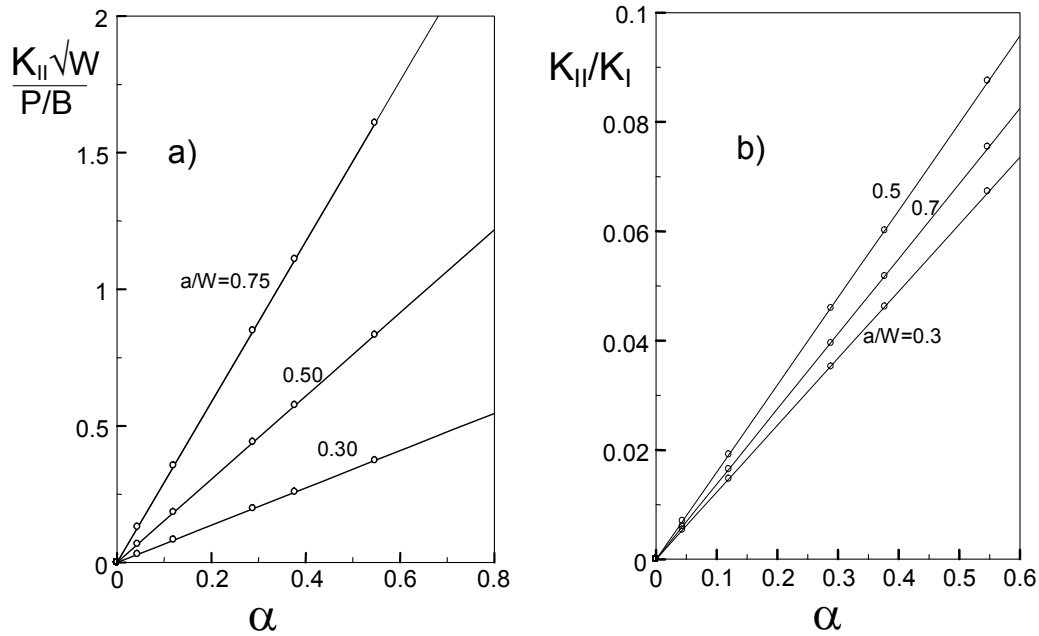


Fig. 16 Stress intensity factor K_I and effective stress intensity factor K_{eff} (representing the energy release rate).



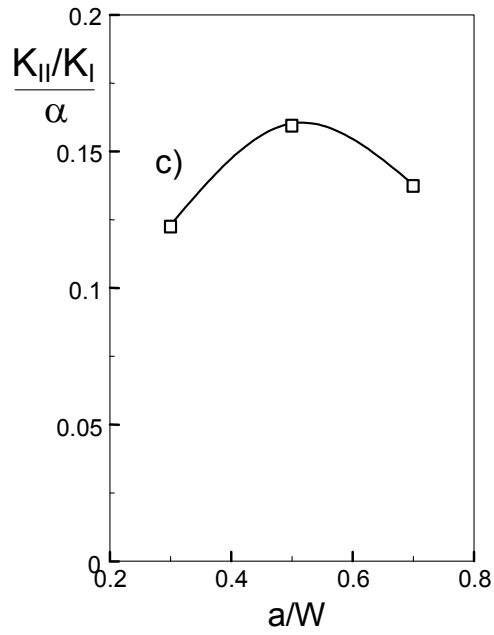


Fig. 17 a) Stress intensity factor K_{II} , b) mode mixity K_{II}/K_I , and c) slope of the mode mixity straight lines in b).

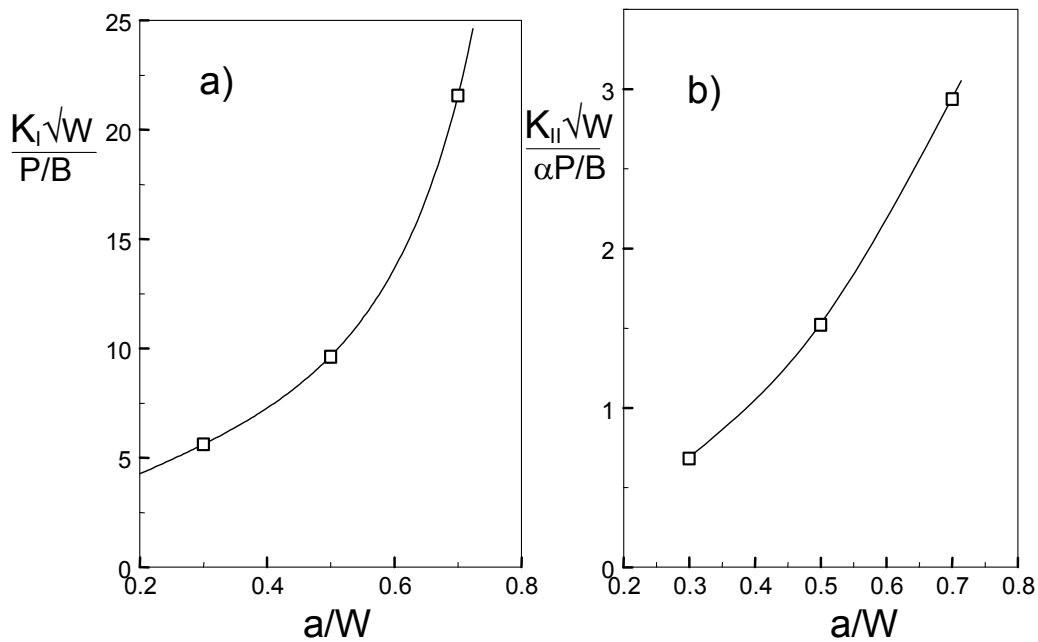


Fig. 18 a) Mode-I stress intensity factor K_I of the homogeneous material ($\alpha=\beta=0$), symbols: FE results, curve: eq.(27) proposed by Srawley [10], b) slope of the straight lines in Fig. 17a.

3.2 Constant stress terms

The two constant x-stress terms σ_{01} and σ_{02} are given in Fig. 19a, normalised to the stress term for $\alpha=0$. This stress of the homogeneous specimen is identical with the T-stress and plotted in Fig. 19b versus the relative crack size a/W . For $a/W < 0.6$ and $\alpha < 0.6$ we propose the relations

$$\sigma_{01} = T(1 + 0.8\alpha) \quad (28)$$

$$\sigma_{02} = T(1 - 0.85\alpha) \quad (29)$$

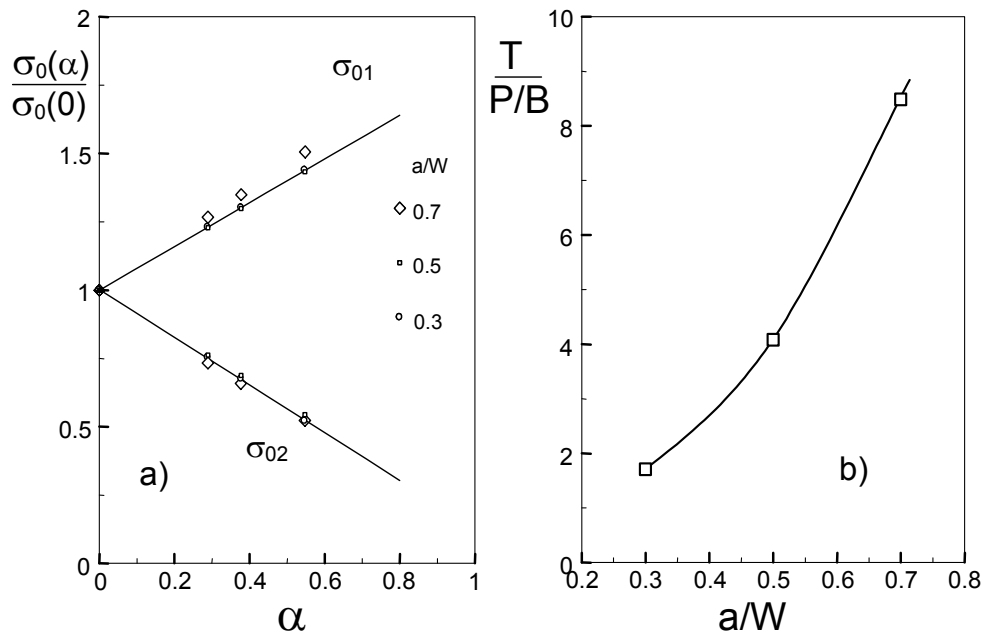


Fig. 19 a) Constant stress terms normalised to the constant stress for homogeneous material at variable ratios a/W ($\beta=0$), straight lines: eqs.(28) and (29), b) constant stress term (T-stress) of homogeneous material versus a/W .

4. DCDC test specimen

The “double cleavage drilled compression” (DCDC) specimen shown in Fig. 20 is used for the determination of stable and subcritical crack growth under mixed-mode loading conditions (e.g. [11-13]).

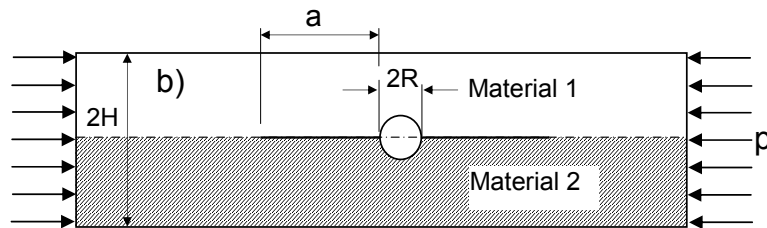


Fig. 20 DCDC specimen with central hole

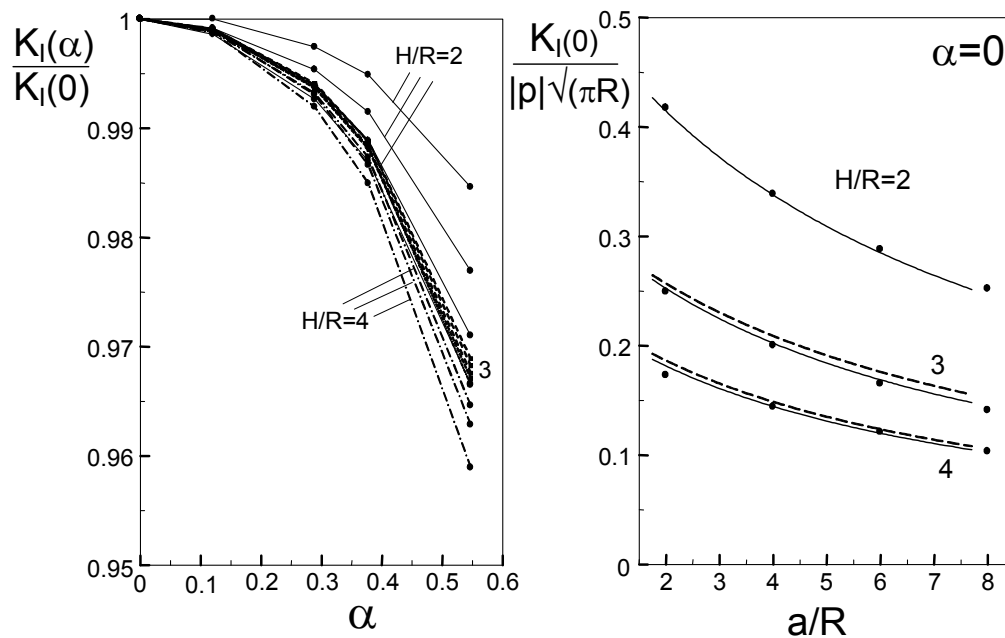


Fig. 21 a) Influence of Dundurs parameter α on K_I , b) stress intensity factor K_I of homogeneous material, circles: this report, dashed curves: eq.(31) [11], solid curves: eq.(32) [14].

Figure 21a shows the mode-I stress intensity factor K_I normalised to the value of homogeneous material (i.e. for $\alpha=\beta=0$) versus α . The plots for $H/R=3$ and 4 may be expressed by the common relation of

$$K_I = K_I(0) \times (1 - 0.107 \alpha^2) \quad (30)$$

For the case of a homogeneous material ($\alpha=\beta=0$), the mode-I stress intensity factor was given by He et al. [11] for $a/R \geq 4$ as

$$\frac{|p|\sqrt{\pi R}}{K_I(0)} = \frac{H}{R} + \left[0.235 \frac{H}{R} - 0.259 \right] \frac{a}{R} \quad (31)$$

This solution is introduced as the dashed curves in Fig. 21b. A solution proposed in [14] reads

$$\frac{|p|\sqrt{\pi R}}{K_I(0)} = 1.1163 \frac{H}{R} - 0.3703 + \left[0.216 \frac{H}{R} - 0.1575 \right] \frac{a}{R} \quad (32)$$

which is represented by the solid curves in Fig. 21b. Equation (30) in combination with (31) or (32) allows to compute the mode-I stress intensity factor for the DCDC specimen made of dissimilar materials.

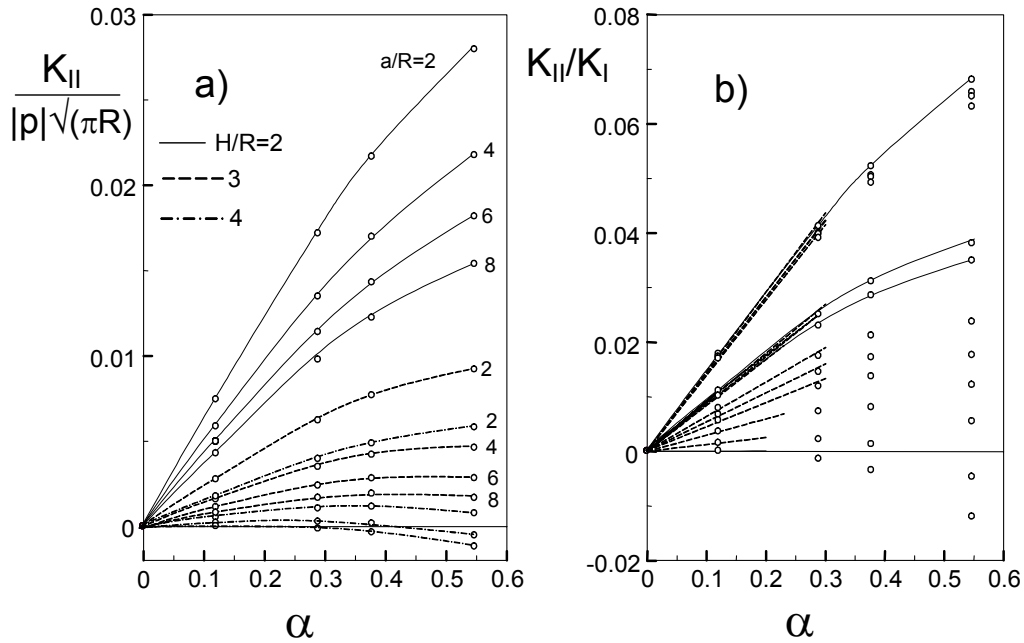


Fig. 22 Mode-II stress intensity factor (a) and mode mixity K_{II}/K_I versus Dunders parameter α .

The mode-II stress intensity factor K_{II} is plotted in Fig. 22a. Figure 22b represents the mode-mixity $K_{II}/K_I=f(\alpha)$. If $\alpha < 0.3$, mode mixity may be approximated by linear relations as

$$K_{II} / K_I = C\alpha \quad (33)$$

with the coefficient C compiled in Table 1.

H/R	$a/R=2$	4	6	8
2	0.145	0.141	0.140	0.138
3	0.0494	0.0630	0.0531	0.0441
4	0.0842	0.0298	0.0126	0

Table 1 Coefficients C for mode mixity according to eq.(33), $\alpha < 0.3$.

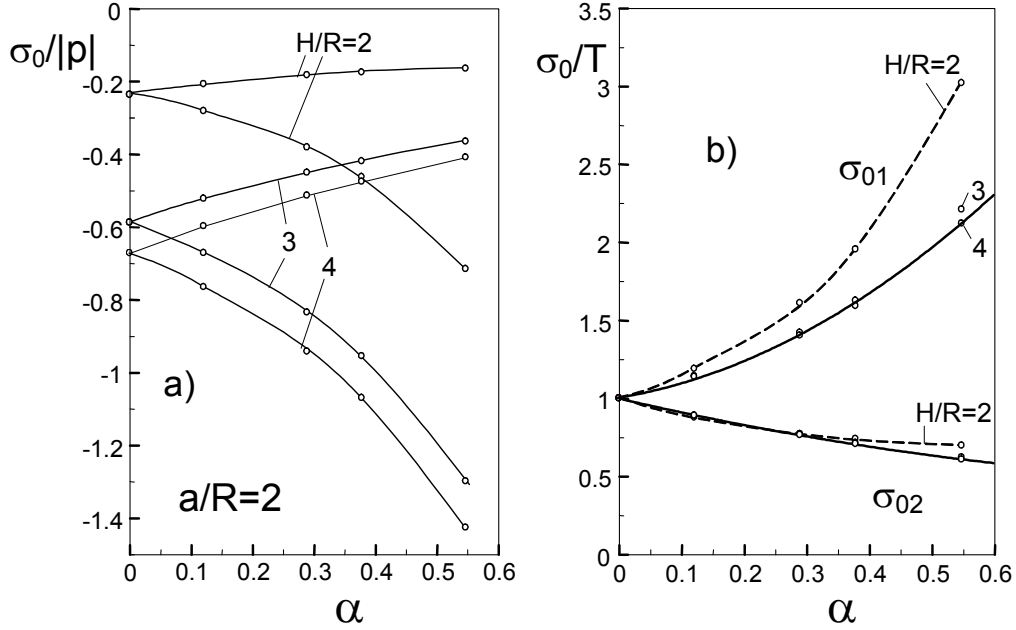


Fig. 23 a) Constant stress terms of the DCDC test specimen, b) normalised to the T-stress.

In Fig. 23 the constant stress terms are plotted for $a/R=2$. At $H/R > 3$ and $\alpha < 0.6$, the constant stresses may be estimated roughly by

$$\sigma_{01}/T \approx 1 + 0.6678\alpha + 2.4987\alpha^2 \quad (34)$$

$$\sigma_{02}/T \approx 1 - 0.9329\alpha + 0.4008\alpha^2 \quad (35)$$

These dependencies are presented as the solid curves in Fig. 23b. The T-stress T for the homogeneous material can be expressed by [14]

$$T/|p| = \frac{1}{1.11H/R - 1.157 + (0.213H/R - 0.283)a/R} - 1 \quad (36)$$

5. Opposite roller test

An experimental set up for a fracture mechanics test with completely stable crack propagation as developed in [15] for homogeneous materials is shown in Fig. 24. A pre-notched bar is loaded via four opposite rollers. The effect of dissimilar materials will be studied below.

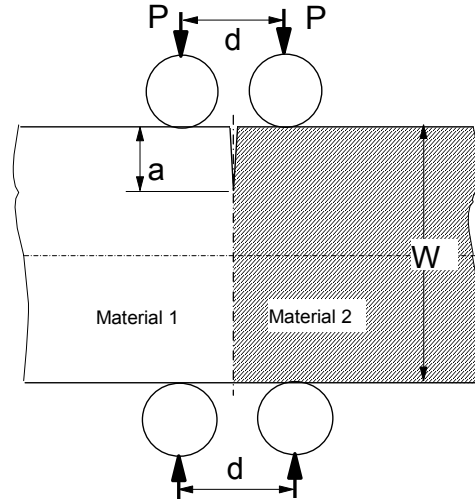


Fig. 24 Controlled fracture test device with load application via four symmetrical rollers.

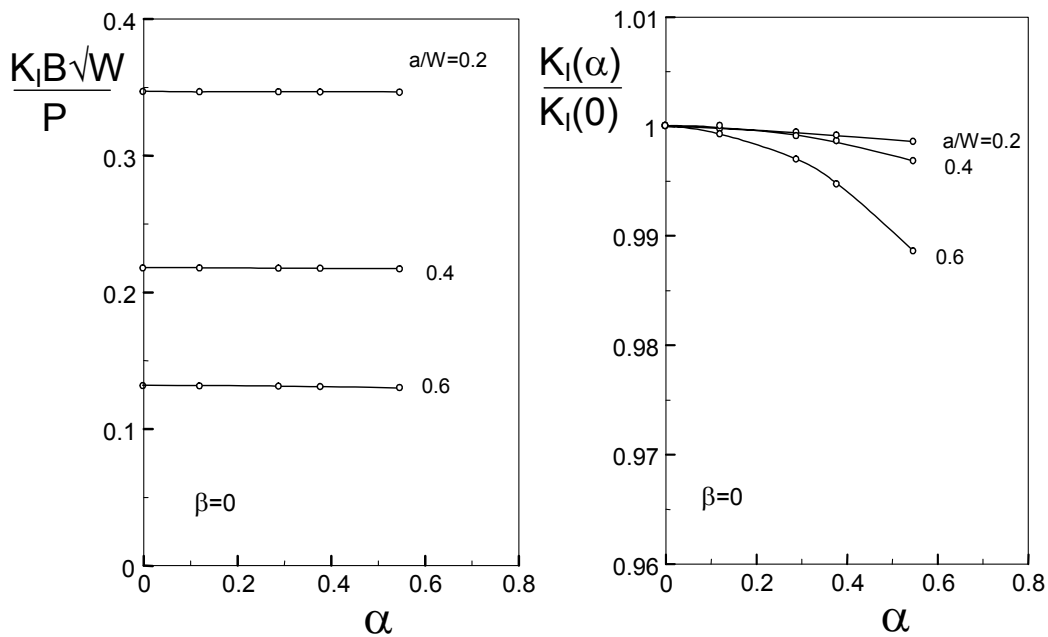


Fig. 25 a) Influence of Dundurs parameter α on K_I , b) normalised representation of a).

Figure 25 represents the mode-I stress intensity factor K_I as a function of the Dundurs parameter α and the relative crack length a/W . From the plot in Fig. 25b, it is clearly visible that the influence of crack length on the normalised stress intensity factor $K_I(\alpha)/K_I(0)$ is negli-

ble. The value of $K_I(0)$ is identical with the stress intensity factor solution for homogeneous material. The solution obtained by the weight function technique reads [15]

$$K_I = \frac{2P}{B\sqrt{W}} (0.905\eta^{1/2} - 3.358\eta^{3/2} + 3.857\eta^{5/2} + 1.4425\eta^{7/2} - 3.873\eta^{9/2}) \quad (37)$$

with $\eta=a/W$. Equation (37) is plotted in Fig. 26 together with the data from the present FE analysis. Good agreement is obvious.

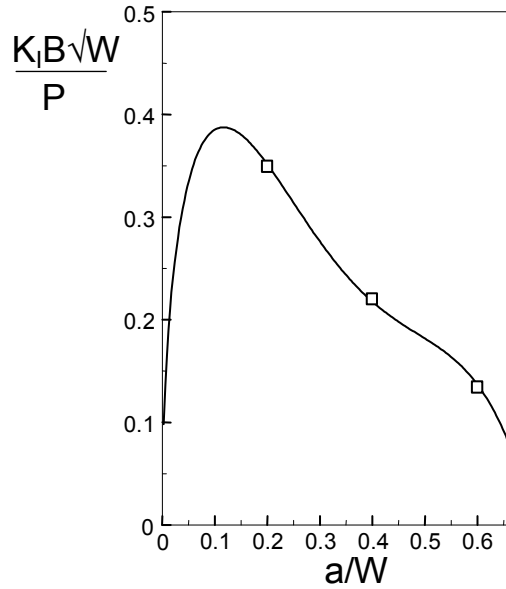


Fig. 26 Stress intensity factor solution for homogeneous material; curve: eq.(37) [15], squares: FE results.

Figure 27 shows the mode-II stress intensity factor as a function of the Dundurs parameter α and the relative crack length a/W . The linear dependencies shown in Fig. 27a can be expressed as

$$K_{II} = C_{II} \frac{P}{B\sqrt{W}} \alpha \quad (38)$$

with the coefficient C_{II} plotted in Fig. 27b versus the relative crack length. Finally, Fig. 27c illustrates the mixed-mode ratio K_{II}/K_I . Since for $a/W=0.2$ and 0.4 the mode-II stress intensity factor is small compared to the mode-I stress intensity factor, it is self-evident that the effective stress intensity factor K_{eff} , representing the energy release rate cannot differ significantly from the mode-I value K_I . Due to this fact, a separate plot of the effective stress intensity factor did not seem to be necessary.

The constant stress terms are given in Fig. 28a. The straight line behaviour may be expressed by the relations

$$\sigma_{0I} = T(1 + C_1 \alpha) \quad (39)$$

$$\sigma_{02} = T(1 - C_2\alpha) \quad (40)$$

The T-stress data obtained with FE are shown by the symbols in Fig. 29. A solution tabulated in [16] and interpolated using cubic splines is entered as the solid curve. Also in this case, good agreement is visible.

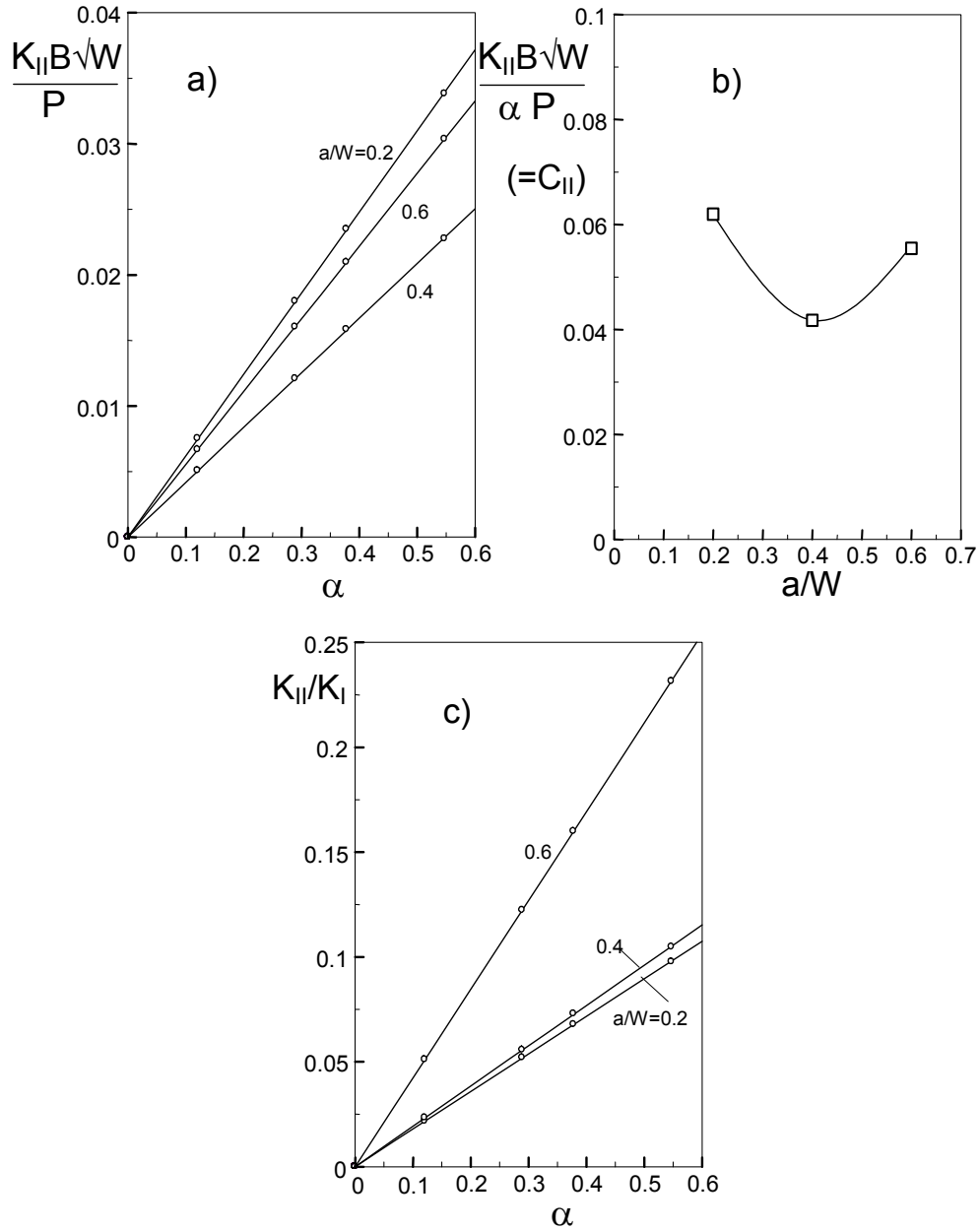


Fig. 27 a) Influence of Dundurs parameter α on K_{II} , b) steepness of the curves of a), c) mixed-mode ratio K_{II}/K_I .

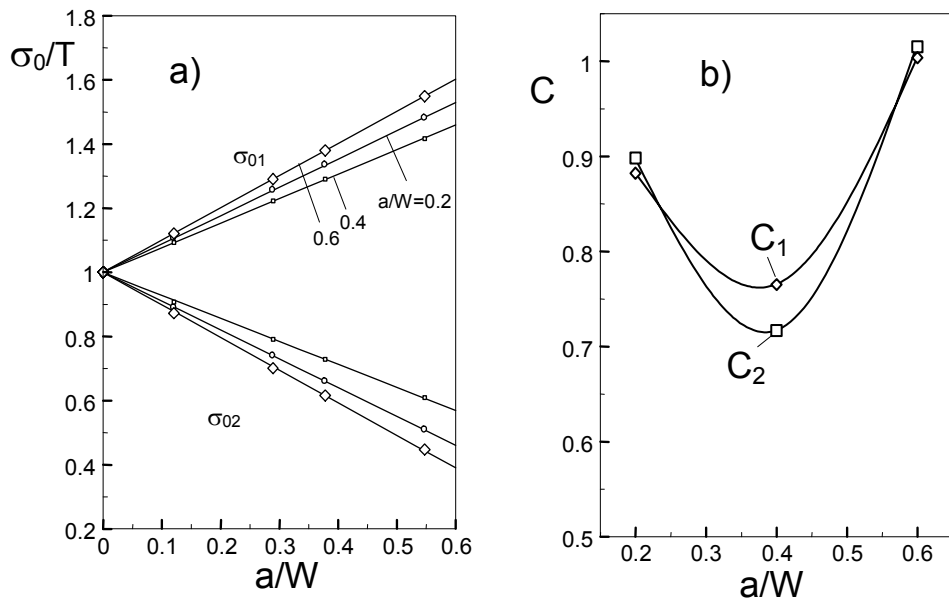


Fig. 28 a) Constant stress terms normalised to the T-stress, b) coefficients for eqs.(39) and (40).

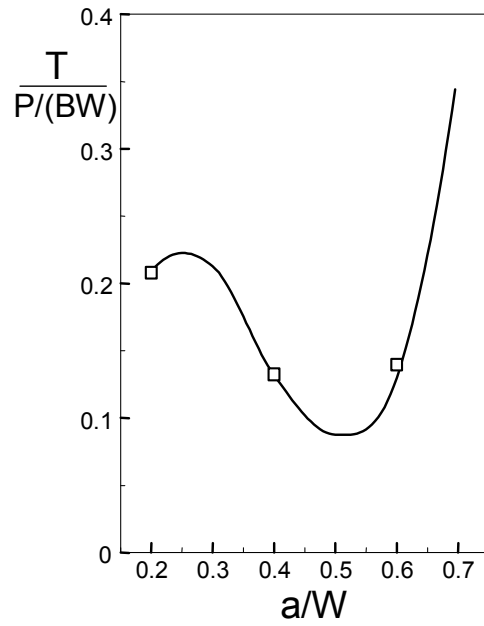


Fig. 29 T-stress from the FE analysis (symbols) compared with a solution tabulated in [16] and interpolated with cubic splines.

6. Bending bar

The bending bar made of dissimilar materials was studied very early. A large number of references is given in [17]. In most papers the energy release rate is considered the driving force in fracture mechanics tests. Therefore, it is here concentrated on the constant stress terms. Figure 30 shows the geometrical data.

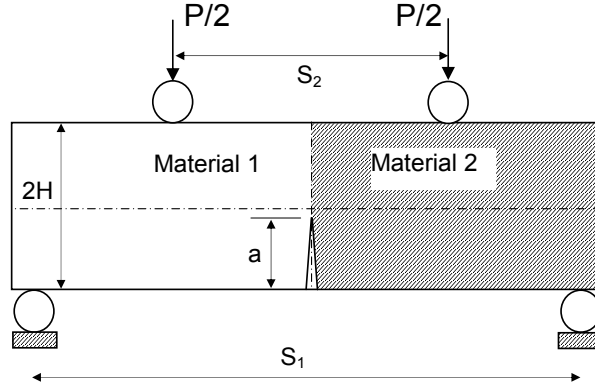


Fig. 30 4-point bending specimen with a crack at the interface.

For the homogeneous test specimen the stress intensity factor and the T-stress are well known. The stress intensity factor K_I is

$$K_I = \sigma_b \sqrt{\pi a} F \quad (41)$$

with the bending stress σ_b

$$\sigma_b = \frac{3P(S_1 - S_2)}{2BW^2} \quad (42)$$

and [8]

$$F = \frac{1.1215}{(1-\eta)^{3/2}} \left[\frac{5}{8} - \frac{5}{12}\eta + \frac{1}{8}\eta^2 + 5\eta^2(1-\eta)^6 + \frac{3}{8}\exp(-6.1342\eta/(1-\eta)) \right] \quad (43)$$

with $\eta=a/W$. This relation is plotted as the curve in Fig. 31a. The squares represent numerical solutions obtained by the finite element computations. Good agreement can be seen. The related T-stress can be expressed by [16]

$$\frac{T}{\sigma_b} = \frac{-0.526 + 2.481\eta - 3.553\eta^2 + 2.6384\eta^3 - 0.9276\eta^4}{(1-\eta)^2} \quad (44)$$

This dependency is plotted as the curve in Fig. 31b. Also in this case, the squares result from FE computations. Best agreement with eq.(44) is evident. In Fig. 32a the mode-I stress intensity factor for the specimen made of dissimilar materials is normalised to the stress intensity factor according to eqs.(41-43) and plotted versus the Dundurs parameter α . The influence of α is negligible for $\alpha < 0.5$. Figure 32b shows the mixed-mode ratio K_{II}/K_I for several relative crack lengths a/W . In Fig. 32c the steepness of the curves K_{II}/K_I vs. α is shown, defining the coefficient λ_1 in

$$K_{II} / K_I = \lambda_1 \alpha . \quad (45)$$

In Fig. 32d the ratio of the effective stress intensity factor K_{eff} (representing the energy release rate via eq.(6)) and the mode-I contribution K_I is plotted. Maximum deviations of less than 0.4% are visible. From this result, it can be concluded that the solution for homogeneous material can be applied for the computation of energy release rates.

The constant stress terms for three crack lengths are plotted in Fig. 33a.

$$\sigma_{01} = T + \lambda_2 \alpha \quad (46)$$

$$\sigma_{02} = T - \lambda_2 \alpha \quad (47)$$

with T given by eq.(44).

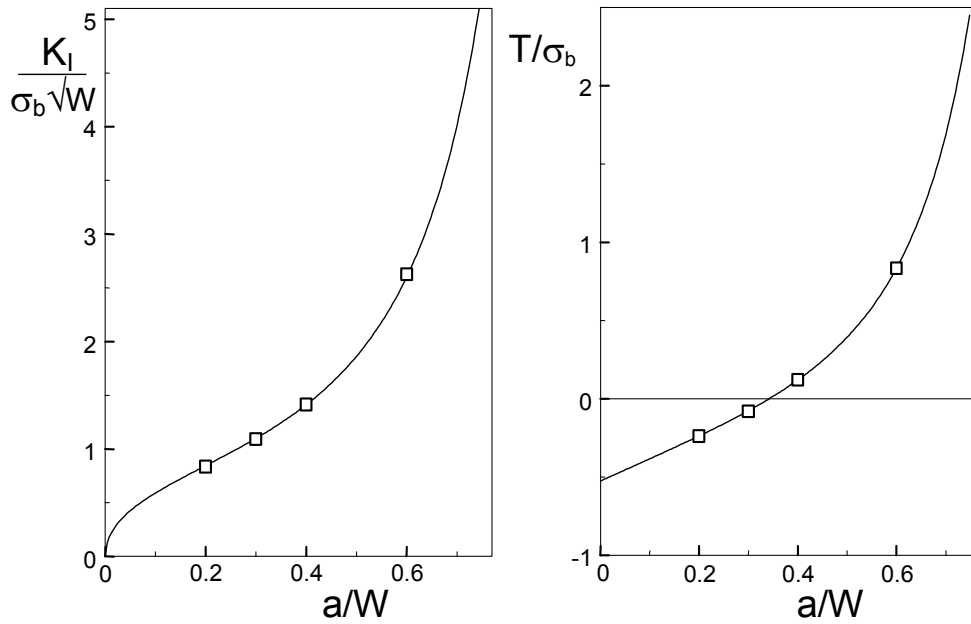


Fig. 31 a) Mode-I stress intensity factor K_I of homogeneous material ($\alpha=\beta=0$), symbols: FE results, curve: eq.(43), b) T-stress solution eq.(44).

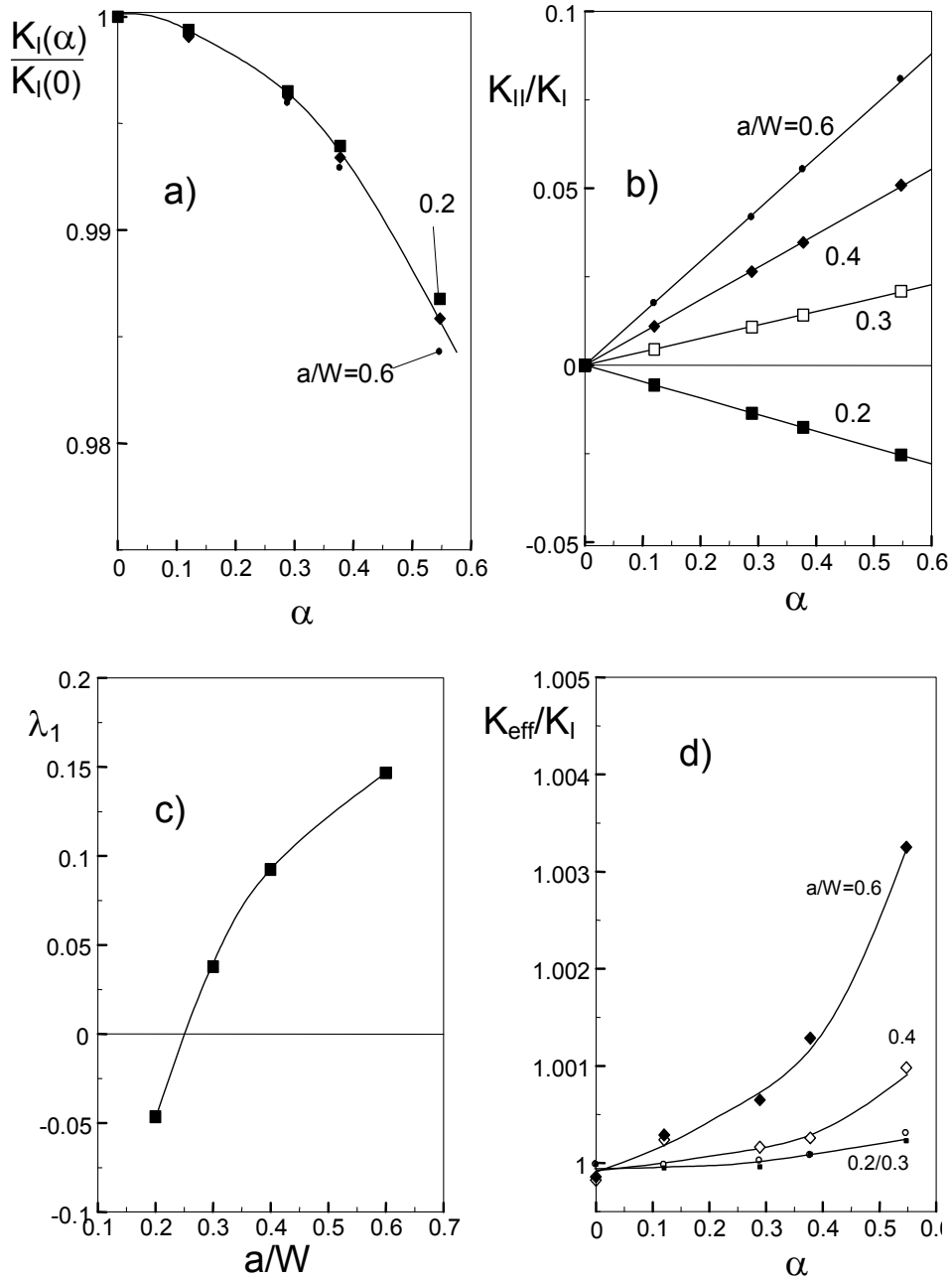


Fig. 32 a) Mode-I stress intensity factor K_I of dissimilar materials, b) mixed-mode ratio, c) slope of the curves in (b), defining the coefficient λ_1 in eq.(45), d) energy release rate expressed by the effective stress intensity factor according to eq.(6).

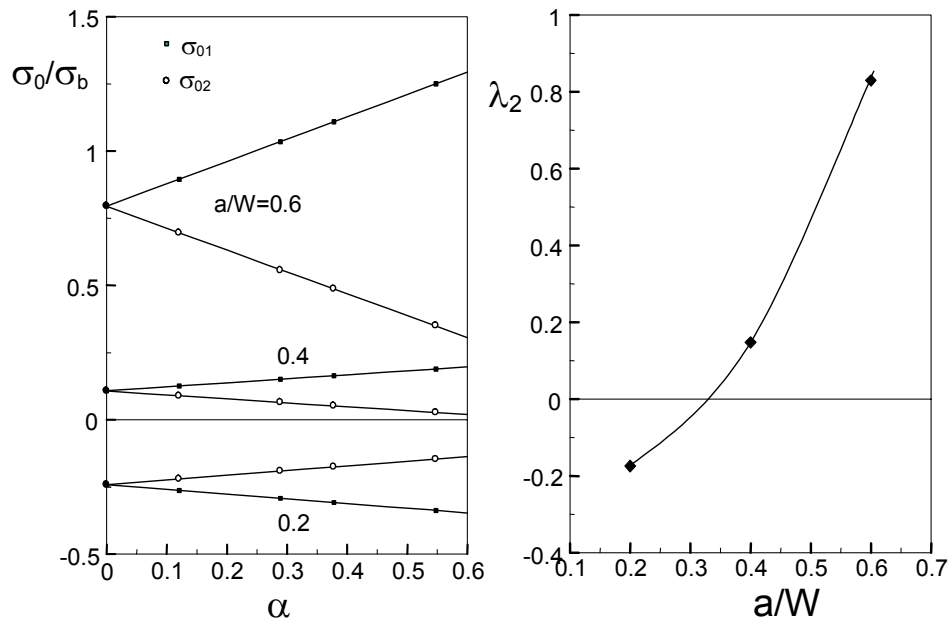


Fig. 33 a) Constant stress terms normalised to the bending stress, b) coefficient λ_2 for eqs.(46) and (47), representing the slopes in (a).

References

- [1] Rice, J.R., Elastic fracture mechanics concepts for interfacial cracks, *J. Appl. Mech.* **55**(1988), 98-103.
- [2] Sih, G.C., Chen, E.P., Cracks in composite materials, Ch.3, (Mechanics of Fracture VI), ed. by G.C. Sih, Martinus Nijhoff Publishers, The Hague (1981).
- [3] He, M.Y., Hutchinson, J.W., Kinking of a crack out of an interface, *J. Appl. Mech.* **56**(1989), 270-278.
- [4] He, M.Y., Bartlett, A., Evans, A.G., Hutchinson, J.W., Kinking of a crack out of an interface: Role of in-plane stress, *J. Am. Ceram. Soc.* **74**(1991), 767-771.
- [5] Cotterell, B., Rice, J.R., Slightly curved or kinked cracks, *Int. J. of Fract.* **16**(1980), 155-169.
- [6] Hutchinson, J.W., Mixed mode fracture mechanics of interfaces, in: *Metal/Ceramic Interfaces*, Ed. by M. Rühle, A.G. Evans, M.F. Ashby, and J.P. Hirth, Pergamon Press, Elmsford, NY, 1990.
- [7] Murakami, Y., Hanson, M.T., Hasebe, N., Itoh, Y., Kishimoto, K., Miyata, H., Miyazaki, N., Terada, H., Tohgo, K., Yuuki, R., *Stress Intensity Factors Handbook*, Vol. 3. Pergamon Press, (1992), Oxford, UK.
- [8] Fett, T., Munz, D. (1997). *Stress Intensity Factors and Weight Functions*, Computational Mechanics Publications, Southampton, UK.
- [9] Fett, T., Rizzi, G., T-stress solutions determined by FE computations, Report FZKA 6937, Forschungszentrum Karlsruhe, Karlsruhe (2004), in preparation.
- [10] Srawley, J.E., Wide range stress intensity factor expressions for ASTM E399 Standard Fracture Toughness Specimens, *Inr. J. Frac. Mech.* **12**(1976), 475-476.
- [11] He, M.Y., Turner, M.R., Evans, A.G., Analysis of the double cleavage drilled compression specimen for interface fracture energy measurements over a range of mode mixities, *Acta metall. mater.* **43**(1995), 3453-3458.
- [12] Ritter, J.E., Huseinovic, A., Chakravarthy, S., Lardner, T.J., Subcritical crack growth in soda-lime glass under mixed-mode loading, *J. Amer. Ceram. Soc.* **83**(2000), 2109-2111.
- [13] Lardner, T.J., Chakravarthy, S., Quinn, J.D., Ritter, J.E., Further analysis of the DCDC specimen with an offset hole, *Int. J. Fract.* **109**(2001), 227-237.
- [14] Fett, T., Rizzi, G., Munz, D., T-stress solution for DCDC specimens, submitted to *Engng. Fract. Mech.*
- [15] Fett, T., Munz, D., Thun, A toughness test device with opposite roller loading, *Engng. Fract. Mech.* **68**(2001), 29-38.
- [16] Fett, T., T-stress and stress intensity factor solutions for 2-dimensional cracks, VDI-Verlag, 2002.

- [17] Suga, T., Bruchmechanische Charakterisierung und Bestimmung der Haftfestigkeit von Materialübergängen, Diss. 1983, Stuttgart